Supplementary material 3

Petrography of the main facies

1. *Biotite granite*

K-feldspar is present as sub- to euhedral crystals (2–5 mm) of perthitic orthoclase and microcline showing a crosshatched twinning. Large crystals usually enclose small plagioclase grains surrounded by a narrow resorption zone.

Plagioclase is represented mainly by interstitial small unzoned albite–oligoclase ($An_{10–11}$). Sometimes oligoclase ($An_{20–24}$) megacrysts (5–7 mm) with oscillatory magmatic zoning show a narrow albite rim (An_{04}). Antiperthitic texture at the contact between K-feldspar and plagioclase is frequently observed; myrmekite rims are rare.

Biotite occurs as unzoned flakes (2–3 mm) which are strongly pleochroic from pale yellow to dark brown. They display low X_{Mg} [$Mg/(Mg + Fe^{2+})$] (0.22–0.32), high Ti (0.33–0.38 apfu) and Al_T (2.9–3.0 apfu) (*Tab. 1 below*). In the X_{Mg}–Al_T classification diagram, the biotites are straddling the boundary between annite and siderophyllite fields (*not shown*). Biotite is sometimes chloritized along cleavage.

Muscovite is usually found as small (~100 μm) flakes enclosed in plagioclase or at the rim of biotite. Rare muscovite grains have subhedral shape and the same grain size as the matrix (2–3 mm). They are poor in Ti (0.038–0.039 apfu) and Na (0.048–0.084 apfu) compared to K (1.92–2.00 apfu), a feature typical of secondary muscovite (Zen 1988).

Accessory phases are dominated by apatite needles. Ilmenite is both primary within the matrix, as well as secondary along biotite cleavage. Monazite is euhedral, equant with a yellow honey colour. Rare allanite was identified, magnetite is absent.

2. *Starost granodiorite*

K-feldspar is represented by homogeneous ($Ab_{5–8}$) or perthitic orthoclase of variable size (0.1–1 mm). K-feldspar oikocrysts containing anhedral to euhedral plagioclase laths and small biotite blades sometimes occur. The K-feldspars exhibit deep marine blue cathodoluminescence (CL) associated with weak continuous zoning, from a light core correlated with higher Na_2O (0.79 wt. %) and BaO (0.52 wt. %), to a darker rim containing a lower proportion of Na_2O (0.53 wt. %) and BaO (0.17 wt. %). Some specimens show complicated zoning as illustrated by Zachovalová et al. (2002). Such complex internal features of K-feldspar phenocrysts have been investigated by Vernon (1986).

Plagioclase is smaller than K-feldspar (~0.5 mm), of oligoclase–andesine composition with normal zoning (cores: $An_{29–32}$, rims: $An_{20–22}$). Smaller crystals in the matrix are of homogeneous oligoclase (~An_{20}) composition. Polysynthetic twinning is rare, cores are usually dusty with secondary sericitization. The andesine cores show light green-blue CL, whereas oligoclase is dull brown-blue.

Biotite occurs as small (~200 μm), interstitial, anhedral flakes with strong pleochroism ranging from yellow-brown to dark brown. They are chemically homogeneous, with slightly higher X_{Mg} (0.33–0.35) and Ti (0.45–0.48 apfu) but lower Al_T (2.48–2.54 apfu) than in the biotite granite, corresponding to annite (*Tab. 1 below*).

Amphibole grains (0.5–1 mm) are anhedral–euhedral, homogeneous and show a strong yellow-brownish to dark-green pleochroism. Titanium content is moderate (0.13–0.14 apfu); X_{Mg} [Mg/(Mg + Fe^{2+})] ranges from 0.38 to 0.46 (*Tab. 2 below*). Because of variable (Na + K) in B site (0.43–0.52), amphiboles are classified as ferro-hornblende to ferro-edenite (Leake et al. 1997). A few large xenocrysts (~3 mm) are compositionally zoned, with a distinct yellow core and green rim in transmitted light (Fig. 1a below). The core of such amphibole has a magnesio-hornblende to edenitic composition, with higher X_{Mg} (0.52–0.55) but stable content of Ti (0.13–0.15), while rim corresponds to ferro-hornblende.

Among *accessory phases*, the most common are short needles and equant grains of apatite, albeit less abundant than in the quartz monzodiorite. Ilmenite occurs as a primary phase within the matrix. Euhedral allanite with orange rim and dark brown metamict core was observed. Monazite and magnetite are absent.

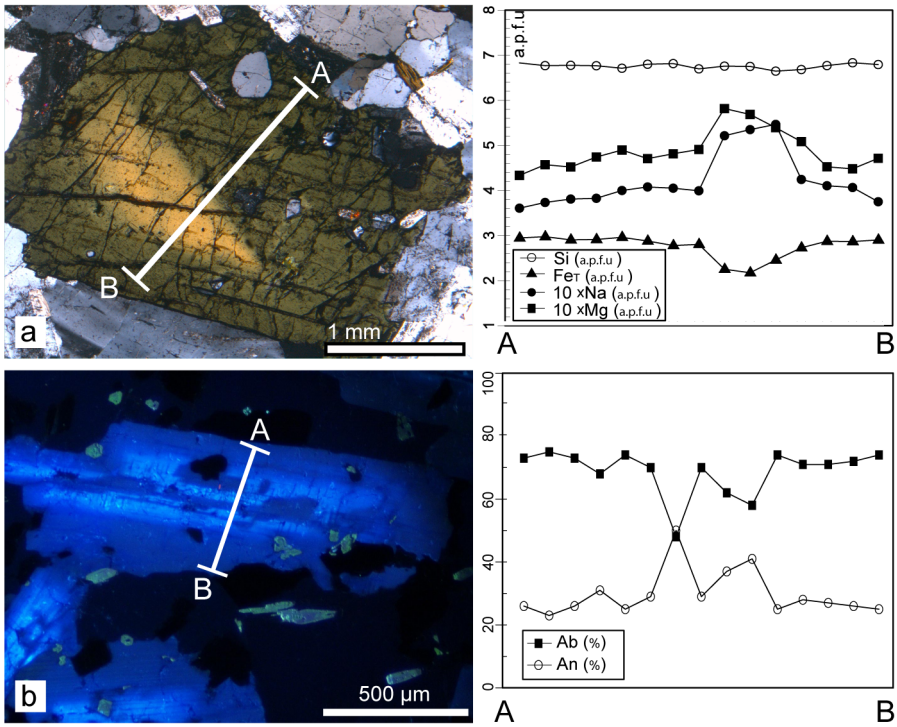

Fig. 4a – Zoned amphibole phenocryst from the Starost granodiorite. A–B compositional profiles in Si, FeT, 10×Na and 10×XMg (a.p.f.u.) **b** – Optical cathodoluminescence image of a discontinuously zoned plagioclase from the quartz monzodiorite (ZU-9). Acquired by the cold-stage CITL CL Mk 5-2 apparatus, under vacuum of 0.003 mbar and operating conditions of ~730 µA and 17 kV.A–B compositional profile in albite (Ab) and anorthite (An) (mol. %).

3. *Quartz monzodiorite*

K-feldspar, when present, is associated with small quartz or occurs as oikocrysts enclosing euhedral plagioclase, biotite and amphibole grains.

Plagioclase forms small euhedral, homogeneous andesine–oligoclase crystals ($An_{23–32}$), mostly with a weak normal zoning. Rarer discontinuously zoned megacrysts (up to 15 mm) contain boxy-cellular or dendritic andesine–labradorite cores ($An_{45–50}$) resorbed and

overgrown by oligoclase rims ($An_{18–25}$) (Fig. 1b above). The oligoclase rims enclose numerous hornblende and biotite inclusions, as well as concentrically aligned angular fragments of the cores. The external shape of plagioclase megacrysts is anhedral, filling the empty space between mafic minerals. The CL colour of plagioclase is marine blue, with light blue cores (see also Zachovalová et al. 2002).

Biotite is euhedral in coarse-grained quartz monzodiorite, where it occurs in aggregates with amphibole, usually overgrown by secondary ilmenite. In the fine-grained facies, biotite is interstitial to euhedral. Both types show a very strong pleochroism, from pale yellow to almost opaque brown, and comparable chemistry: X_{Mg} (0.35–0.40), Al_T (2.43–2.54 apfu) and Ti (0.43–0.60 apfu) (Tab. 1 below). Interestingly, the biotite is almost devoid of pleochroic haloes, unlike in granite and granodiorite.

Amphibole is represented by pleochroic, green to yellow ferro-hornblende to magnesio-hornblende with euhedral to subhedral shapes. In fine-grained quartz monzodiorites, amphiboles have roughly the same composition as in the Starost granodiorite, with somewhat higher Ti contents (0.15–0.19 apfu). In contrast, magnesio-hornblendes from coarse-grained quartz monzodiorites show significantly lower Al_T (0.90–1.18 apfu) and Ti (0.06–0.11 apfu) (Tab. 2 below).

In our dataset, only three magnesio-hornblendes from the quartz monzodiorite ZU-6 were in textural equilibrium with the matrix and fall in the calibration range of the geothermobarometer by Ridolfi and Renzulli (2012). Calculated P–T conditions are 758 ± 22 °C and 100 ± 11 MPa (Tab. 2 below).

Sphene may represent up to 3 vol. % of the rock but usually does not exceed 1 vol. %. The fine-grained quartz monzodiorite shows a macroscopically well-developed sphene-centred ocellar texture consisting of leucocratic ocelli with brownish sphene crystals at the centre, enclosed in a biotite-rich matrix (Vegas et al. 2011).

The most frequent a*ccessory mineral* is predominantly needle-shaped apatite (up to ~1 vol. %). The CL reveals a weak internal zoning, from yellow core to brown rim. Ilmenite is the most frequent opaque phase. Strongly metamict allanite with an ilmenite rim is also present. Secondary chlorite after biotite, patchy epidote replacing hornblende, and sericite along plagioclase cleavage, were observed.

Mineral chemistry

Mineral analyses were carried out using a CAMECA SX-100 electron microprobe, housed at the Geological Institute of the Czech Academy of Science, Prague, and equipped with four crystal spectrometers, SE and BSE detector. The microprobe was operated at an accelerating voltage of 15 kV with a beam current of 10 nA and a diameter of 2 μm. Feldspar and biotite analyses were recalculated on the basis of 8 and 22 oxygen atoms, respectively. Amphibole formulae were obtained on the basis of 23 oxygen atoms with Fe^{2+}/Fe^{3+} ratio estimated by adjusting the sum (Si + Al + Cr + Ti + Fe + Mg + Mn) to 13.

Sample	ZU-3	ZU-14	ZU-17	ZU-6	ZU-6	ZU-9
Rock-type	Bt granite	Bt granite	Starost gd	Q mnzd	Q mnzd	Q mnzd
SiO_2	36.53	35.20	36.15	36.26	36.42	36.02
TiO_2	3.93	2.79	3.91	3.99	3.85	3.63
Al_2O_3	13.87	15.98	13.46	13.19	13.18	13.69
FeO	24.91	23.95	25.56	22.90	22.75	24.31
MnO	0.52	0.59	0.34	0.36	0.29	0.23
MgO	6.79	6.46	6.95	8.71	8.25	7.78
CaO	0.07	0.07	0.05	0.01	0.02	0.00
Na_2O	0.06	0.08	0.04	0.09	0.09	0.07
K_2O	9.89	9.80	9.73	9.77	9.78	9.94
SrO	0.00	0.00	0.00	0.00	0.00	0.00
BaO	0.07	0.034	0.11	0.13	0.19	0.369
Rb_2O	0.03	0.11	0.05	0.00	0.00	0.00
Total	96.66	95.05	96.37	95.41	94.82	96.04
Si	5.59	5.55	5.66	5.66	5.72	5.65
Al^{iv}	2.41	2.45	2.33	2.33	2.28	2.34
Al^{vi}	0.49	0.53	0.15	0.10	0.16	0.17
Ti	0.37	0.33	0.46	0.47	0.46	0.43
Fe	3.64	3.16	3.35	2.99	2.99	3.19
Mn	0.07	0.08	0.05	0.05	0.04	0.03
Mg	1.04	1.52	1.63	2.03	1.93	1.81
Y total	5.60	5.61	5.63	5.65	5.58	5.64
Ca	0.005	0.011	0.008	0.002	0.004	0.001
Na	0.007	0.024	0.013	0.028	0.026	0.022
K	1.941	1.972	1.946	1.950	1.961	1.986
Ba	0.004	0.002	0.007	0.008	0.012	0.023
Rb	0.012	0.011	0.005	0.000	0.000	0.000
X total	1.97	2.02	1.98	1.99	2.00	2.03
OH*	4	4	4	4	4	4
Total	19.57	19.63	19.61	19.63	19.59	19.66
XMg	0.22	0.32	0.33	0.40	0.39	0.36
Al^{tot}	2.90	2.97	2.49	2.43	2.44	2.51
Al^{vi} / Al^{tot}	0.17	0.18	0.06	0.04	0.07	0.07

Tab. 1: Chemical composition of representative biotites (wt. %; a.p.f.u.). Bt granite = biotite granite, Starost gd = Starost granodiorite, Q mnzd = quartz monzodiorite.

Sample	ZU-17	ZU-17	ZU-6	ZU-6	ZU-6	ZU-6	ZU-6	ZU-9.1	ZU-9.1
Rock-type	Starost gd	Starost gd	Q mnzd	Q mnzd	Q mnzd	Q mnzd	Q mnzd	Q mnzd	Q mnzd
SiO_2	43.46	45.21	47.06	46.86	47.17	48.96	49.37	44.26	44.32
TiO_2	1.16	1.31	0.84	0.90	1.01	0.42	0.57	1.37	1.56
Al_2O_3	8.29	9.05	6.63	6.42	6.30	5.22	5.13	8.67	8.42
Cr_2O_3	0.01	0.00	0.00	0.04	0.04	0.01	0.02	0.03	0.04
Fe_2O_3	3.57	1.78	1.69	3.21	1.79	1.63	2.20	1.32	0.65
FeO	19.47	15.82	17.11	16.55	17.23	17.16	16.97	20.35	20.75
MnO	0.89	0.52	0.56	0.49	0.30	0.49	0.59	0.43	0.36
MgO	6.81	10.18	9.96	9.80	9.95	10.47	10.15	7.44	7.56
CaO	11.23	11.66	11.86	11.64	11.78	12.08	11.52	11.72	11.81
Na_2O	1.37	1.96	1.03	1.04	0.98	0.75	0.88	1.27	1.25
K_2O	1.07	0.57	0.78	0.70	0.65	0.50	0.52	1.06	1.10
BaO	0.01	0.00	0.04	0.00	0.03	0.00	0.02	0.04	0.02
F	0.00	0.00	0.00	0.00	0.00	0.00	0.00	0.00	0.00
Cl	0.06	0.00	0.04	0.04	0.05	0.02	0.05	0.07	0.10
Total	97.02	97.90	97.43	97.32	97.04	97.52	97.75	97.87	97.84
Si	6.73	6.75	7.08	7.05	7.11	7.31	7.35	6.77	6.79
Al^{iv}	1.27	1.25	0.92	0.95	0.89	0.69	0.65	1.23	1.21
Al^{vi}	0.24	0.35	0.26	0.19	0.23	0.23	0.25	0.33	0.31
Ti	0.13	0.15	0.10	0.10	0.11	0.05	0.06	0.16	0.18
Cr	0.00	0.00	0.00	0.00	0.00	0.00	0.00	0.00	0.00
Fe^{3+}	0.42	0.20	0.19	0.36	0.20	0.18	0.25	0.15	0.08
Fe^{2+}	2.52	1.98	2.15	2.08	2.17	2.14	2.11	2.60	2.66
Mn	0.12	0.07	0.07	0.06	0.04	0.06	0.07	0.06	0.05
Mg	1.57	2.27	2.23	2.20	2.24	2.33	2.25	1.70	1.73
Ca	1.86	1.87	1.91	1.88	1.90	1.93	1.84	1.92	1.94
Na	0.41	0.57	0.30	0.30	0.29	0.22	0.25	0.38	0.37
K	0.21	0.11	0.15	0.13	0.13	0.10	0.10	0.21	0.21
Sum of cations	15.48	15.54	15.36	15.31	15.32	15.25	15.19	15.50	15.52
Sum OH site	2.00	2.00	2.00	2.00	2.00	2.00	2.00	2.00	2.00
$Mg/(Mg+Fe^{2+})$	0.38	0.53	0.51	0.51	0.51	0.52	0.52	0.39	0.39
Al^{tot}	1.51	1.59	1.18	1.14	1.12	0.92	0.90	1.56	1.52
$Fe^{3+}/(Fe^{2+}+Fe^{3+})$	0.14	0.09	0.08	0.15	0.09	0.08	0.10	0.06	0.03
Na + K	0.48	0.69	0.36	0.31	0.32	0.25	0.19	0.50	0.52
T (°C)	–	–	764	757	754	–	–	–	–
Uncertainty (2σ)	–	–	22	22	22	–	–	–	–
P (MPa)	–	–	105	99	96	–	–	–	–
Uncertainty (2σ)	–	–	12	11	11	–	–	–	–

Tab. 2: Chemical composition of representative amphiboles (wt. %; a.p.f.u.) and hornblende geothermobarometry after Ridolfi and Renzulli (2012). Abbreviations as in Tab. 1

References

Leake BE, Wooley AR, Arps CES, Birch WD, Gilbert MC, Grice JD, Hawthorne FC, Kato A, Kisch HJ, Krivovichev VG, Linthout K, Laird J, Mandarino JA, Maresch WV, Nickel EH, Rock NMS, Schumacher JC, Smith DC, Stephenson NCN, Ungaretti L, Whittaker EJW, Guo Y (1997) Nomenclature of amphiboles: report of the Subcommittee on Amphiboles of the International Mineralogical Association, Commission on New Minerals and Mineral Names. Canad Mineral 35: 219–246

Ridolfi F, Renzulli A (2012) Calcic amphiboles in calc-alkaline and alkaline magmas: thermobarometric and chemometric empirical equations valid up to 1,130°C and 2.2 GPa. Contrib Mineral Petrol 163: 877–895

VEGAS N, RODRIGUEZ J, CUEVAS J, SIEBEL W, ESTEBAN JJ, TUBÍA JM, BASEI M (2011) The sphene-centered ocellar texture: an effect of grain-supported flow and melt migration in a hyperdense magma mush. J Geol 119: 143–157

VERNON R H (1986) K-feldspar megacrysts in granites – phenocrysts, not porphyroblasts. Earth Sci Rev 23: 1-63

ZACHOVALOVÁ K, LEICHMANN J, ŠVANCARA J (2002) Žulová Batholith: a post-orogenic, fractionated ilmenite–allanite I-type granite. J Geosci 47: 35–44

ZEN E (1988) Phase relations of peraluminous granitic rocks and their petrogenetic implications. Ann Rev Earth Planet Sci 16: 21–51